SPECIAL ISSUE

Inversion of Time-Lapse Electric Potential Data to Estimate Fracture Connectivity in Geothermal Reservoirs

Lilja Magnusdottir · Roland N. Horne

Abstract An inverse modeling approach was developed to characterize fracture connectivity in geothermal reservoirs using an injection of a conductive fluid and time-lapse electric potential measurements. Discrete fracture networks with sparsely connected fractures were modeled and a flow simulator was used to solve electric fields as a conductive tracer flows through the fracture networks. The electric potential difference between well pairs drops progressively in time as the conductive fluid fills interconnected fractures along paths from the injector toward the producer. Therefore, the fractional connected area of reservoirs could be estimated using inverse modeling to match the response to other fracture networks by comparing time histories of the electric potential. This method was compared to estimating fractional connected area using tracer return curves alone and the study showed that locations of connected areas were estimated better using the electric potential approach. A sensitivity analysis was performed to study the effect of fractional connected area on time-lapse electric potential and tracer return data. The study verified the advantages of using electric potential measurements instead of only the tracer return curves.

Keywords Fracture characterization · Time-lapse resistivity · Tracer tests · Inverse analysis

1 Introduction

Connectivity of fractures in both natural and enhanced geothermal systems (EGS) is a key factor in interpreting fracture flow, to ensure adequate supply of geothermal

L. Magnusdottir (✉) · R. N. Horne
Department of Energy Resources Engineering, Stanford University,
367 Panama St., Stanford, CA 94305, USA
e-mail: liljam@stanford.edu

fluids and efficient thermal operation of the wells. The interconnected conductive fractures control mass and heat transport in the system and inappropriate placement of injection or production wells can lead to premature thermal breakthrough. Such premature thermal breakthroughs have occurred in numerous geothermal reservoirs, as described by Horne (1983), and observed in The Geysers (Beall et al. 1994). In previous work, chemical tracers have been used to investigate connectivity between wells to prevent premature thermal breakthrough (Fossum and Horne 1982; Fukuda et al. 2006). By injecting a slug of tracer, Shook (2001) showed how tracer histories could be transformed into predicted temperature histories in heterogeneous porous media but the method's accuracy degraded in the presence of a strong permeability correlation. Wu et al. (2008) predicted enthalpy production in fractured geothermal reservoirs using a single fracture model which was also expanded to a two-phase flow scenario in a network of multiple fractures. Analysis of tracer data yielded fracture properties that were used to simulate the enthalpy production but the fracture network contained only parallel vertical fractures. Other methods include using assumptions of specific flow channels connecting injection and production wells with tracer tests to predict premature thermal breakthrough (Axelsson et al. 2005). Such methods can be powerful during early stages of production but more complex models are needed where the flow mechanism is highly complicated. Thus, tracer testing is a potentially powerful technique but accurate interpretation of tracer results in highly fractured reservoirs can be difficult.

Application of geophysical methods has been useful for obtaining physical parameters of the earth system including temperature, elastic properties, density, magnetic susceptibility, and electric conductivity. Conventional wellbore-based techniques for characterizing flow in the subsurface include core sample analysis and well logging. These techniques can give information about the rock type, porosity, and temperature but do not provide information about key controls on overall subsurface flow behavior in fractured reservoirs. Seismic surveys have been used to identify boundaries between flow units in aquifer systems (Chen et al. 2010; Parra et al. 2006) but depth constraints were necessary to reduce uncertainty. Thus, seismic surveys can be useful to study shallow aquifers but it is challenging to detect small-scaled fractures at greater depths. Jeannin et al. (2006) detected fractures in rocks using ground-penetrating radar (GPR) that uses electromagnetic radiation to detect reflected signals from subsurface structures but the antennae reached a maximum penetration of 20 m. Garg et al. (2007) described how self-potential, magnetotelluric and direct current surveys were all used to explore the Beowawe geothermal field in the Basin and Range Province of the western USA. These exploration techniques are commonly used to find hidden geothermal resources that lack hydrothermal surface features, identify promising drilling targets and to help designing recovery strategies appropriately (Harthill 1978; Hochstein and Hunt 1970). They can provide valuable information regarding properties in the subsurface but the relationship between hydraulic and geophysical properties might not be known. In addition, when these geophysical surveys are performed at the surface they do not offer a high level of resolution when exploring deeper portions of the reservoirs, making it challenging to characterize fractures that are small-scaled as compared to the size of the reservoir.

A variety of approaches have been attempted to combine multiple geophysical methods to better quantify hydrological properties in the subsurface (e.g., Garambois et al. 2002). Other approaches include using time-dependent geophysical data that can indirectly measure time-varying hydrologic parameters (Hubbard et al. 2001). Electrical resistivity has been shown to be sensitive to changes in fluid conductivity and water content in reservoirs (Binley et al. 2002; Yeh et al. 2002), and the concentration of a conductive tracer can be mapped from field measurements of resistance using cross-well electrical resistivity tomograpy (ERT) (Singha and Gorelick 2006). A number of studies have demonstrated the potential of ERT for monitoring tracer migration in soil (Binley et al. 1996; Koestel et al. 2008; Olsen et al. 1999; Slater et al. 2002), and in shallow aquifers (Cassiani et al. 2006; Oldenborger et al. 2007; Singha and Gorelick 2005; Singha et al. 2007). In these studies, usually many electrodes were used to obtain the resistivity distribution for the whole field under study at each time step and then this resistivity distribution was ompared to the distribution without any tracer to observe resistivity changes in each block visually. Using this approach for a whole reservoir would require a massive parameter space and likely not be solvable, xcept at very low resolution. Day-Lewis et al. (2003) demonstrated the benefits of time-lapse inversion of geophysical data over the previously mentioned conventional snapshot approach. Lambot et al. (2004) showed how ground-penetrating radar (GPR) was used with hydrodynamic inverse modeling to identify effective hydraulic properties of sand in laboratory conditions. Irving and Singha (2010) have demonstrated an attempt to use Bayesian Markov-chain-Monte-Carlo (McMC) methodology to jointly invert dynamic cross-well and surface resistivity data with tracer concentration data to estimate hydraulic conductivities in heterogeneous geological environments. They concluded that using resistivity data instead of tracer data alone was worth the most where flow was controlled largely by highly connected flow paths (i.e., paths with mean hydrolic conductivity equal to 100 m/d). These methods provided a potential framework for estimating hydraulic properties but none of them was used to characterize fracture networks representing common geothermal reservoirs, which is the focus of the work presented in this paper.

The objective of this study was to find ways to characterize fracture connectivity that could be used to increase the efficiency of fractured geothermal systems and prevent thermal breakthrough. Electrodes were placed inside the wells to measure the resistivity more accurately in the deeper part of the reservoir. The electric potential difference, which corresponds to apparent resistivity, was measured and plotted as a function of time while a conductive tracer was injected into the reservoir. That response, that is potential difference versus time, as the conductive fluid flows through the fracture network, was then used in an inverse modeling process to estimate the connectivity of the reservoir.

Various approaches have been attempted to quantify fracture connectivity, for example using percolation theory (Berkowitz 1995) or the connectivity index approach (Xu et al. 2006). Field studies by Rouleau and Gale (1985) suggest that fracture connectivity is dependent on fracture orientation, spacing and fracture length data but connectivity has also been quantified by the size of a group of linked fractures, known as a cluster (Stauffer 1985). The cluster size is measured by the length of the largest

connected group of fractures as a proportion of the total fracture length in the network (Odling 1997). Alternatively, the connectivity can be defined by the fractional connected area (FCA) which is the fraction of the total area that is connected by clusters, as described by Ghosh and Mitra (2009). In this project, the connectivity was characterized by the FCA because it provides a good indicator of the overall fracture density and does not relate the cluster size to only the connectivity within the largest cluster.

Aside from estimating connected areas another key difference between this and previously related efforts is the small number of electrodes that would be used. One electrode was placed inside each well, so a total of four electrodes were used to estimate the connectivity of a two-dimensional plane. A three-dimensional model could be necessary to model the flow through natural three-dimensional fracture patterns but due to computational complexity it was not considered in this study. If a fracture connecting an injector and a producer is inclined with respect to a two-dimensional plane, only a part of the fracture would be included in the two-dimensional plane. However, the electric current would flow through the most conductive path and indicate a connection between the injector and the producer. Thus, the electric measurements would correspond to the true fracture pattern in the reservoir but the two-dimensional plane under study might not be represented correctly.

The following section first describes how fractal fracture networks that represent the fracture dominated flow in geothermal reservoirs were generated and how a flow simulator was used to simulate the flow of a conductive tracer through the reservoirs. The flow simulator was applied to solve the electric fields at each time step by utilizing the analogy between Ohm's law and Darcy's law. Then, the results are given for when the reservoir response was compared to a library of responses of fracture networks in an inverse analysis to estimate the FCA, by finding the fracture network that matches the reservoir response when time-lapse electric potential data are compared. The relationship between the fracture network and the reservoir response was investigated by comparing the FCA and by visually comparing the similarities between the best match and the true fracture pattern. This approach was also compared to only using tracer data at the producers. In addition, the effects of FCA on both time-lapse electric potential and tracer return curves were studied in a sensitivity analysis.

2 Methodology

A series of simulations were conducted on fractal fracture networks using the general purpose research simulator (GPRS) developed at Stanford University (Cao 2002). GPRS was first used to solve the flow of a conductive tracer and then applied to solve the time-varying electric field. The objective was to investigate the influence of connectivity on the electric potential between well pairs to study the possibility of using changes in electric potential with conductive tracer injection to characterize fracture connectivity. In this section, properties used in GPRS simulation are provided and the generation of fractal fracture networks is described. The definition of FCA is given and the inverse analysis process used in this study is explained.

2.1 Simulation Using GPRS

The GPRS was used to simulate the flow of a conductive tracer through discrete fracture networks (DFN). A DFN approach introduced by Karimi-Fard et al. (2003) was used to create realistic fracture networks where unstructured control volume finite-difference formulation was used with element connections assigned using a connectivity list. Commonly, the physical properties of the fracture networks are upscaled to numerical blocks but this study focused on DFN simulations to avoid volume averaging that would not represent the fracture flow system accurately. Generally, DFN can capture a wider range of transport phenomena. For example, the flow behavior in a matrix with a small number of large-scale fractures which may dominate the flow is represented better with a discrete fracture network (DFN) because the fracture permeability would be underestimated when averaged over grid blocks.

The computational grid was formed using Triangle, a triangular mesh generator developed by Shewchuk (1996). The conductive tracer was chosen to be a NaCl solution and the resistivity of the solution was calculated using a three-dimensional regression formula established by Ucok et al. (1980). Then, the resistivity of the water saturated rock, ρ, was calculated using Archie's law (Archie 1942),

$$\rho = a\phi^{-b}\rho_w \tag{1}$$

where ϕ is the porosity of the rock and a and b are empirical constants. Archie (1942) concluded that for typical sandstones of oil reservoirs the coefficient a is approximately 1 and b is approximately 2 but Keller and Frischknecht (1996) showed that this power law is valid with varying coefficients based on the rock type. In this case, a was set as 0.62 and b as 1.95, which corresponds to well-cemented sedimentary rocks with porosity 5–25 % (Keller and Frischknecht 1996).

For the fracture network examples used in this study, one injection and three production wells were modeled. Water was injected at the rate of 10 kg/s and tracer was 22 wt% of the water injected. The fractures were modeled to be filled with water before any tracer was injected into the reservoir so the initial tracer mass was set to 0.05 wt%. The production well was modeled to deliver against a bottom-hole pressure of 10^6 Pa with a productivity index of 4×10^{-12} m^3. The initial pressure was set to 10^6 Pa and the temperature to 25 °C. The porosity of the fractures was defined as 0.9 and the permeability was determined by

$$k = \frac{w^2}{12} \tag{2}$$

where w is the aperture of the fractures. The matrix blocks were given a porosity value of 0.1 and the permeability was set as 1×10^{-10} m^2. After using GPRS to solve for the tracer flow, the analogy between Darcy's law and Ohm's law (Muskat 1932) was utilized and GPRS used to also solve the electric field as demonstrated earlier by Magnusdottir and Horne (2012).

2.2 Fractal Fracture Networks

Several field studies performed on fault systems at different length scales have demonstrated that fracture populations can follow a power-law length distribution (Shaw and Gartner 1986; Main et al. 1990). Therefore, the length distribution of the fractures can be described by the fractal equations (Nakaya et al. 2003),

$$N(l) = Bl^{-c} \tag{3}$$

$$c = \lim_{l \to 0} \frac{\log N(l)}{\log(1/l)} \tag{4}$$

$$B = (l_{\max})^c \tag{5}$$

where c is the power-law exponent for the fracture length distribution, $l_{\max}$ is the maximum fracture length, and $N(l)$ is the cumulative fracture length distribution, that is the number of fractures with lengths larger or equal to l. Thus, l is equal to $l_{\max}$ when $N(l)$ is equal to 1.

The relationship between the fractal dimension D within an $L \times L$ square domain and $N(r)$, the number of boxes of size r that include the center point of fractures, can also be represented by a fractal equation using the box-counting approach (Barton and Larsen 1985),

$$D = \lim_{r \to 0} \frac{\log N(r)}{\log(1/r)} \tag{6}$$

where $r = L/k$ ($k = 1,2,3,\dots$). The spatial fractal dimension can also be estimated using different techniques such as the sand-box technique. In the sand-box method, the number of fracture center points located inside a circle with a specific center is counted. Then, the size of the circle is increased and the same procedure continued. Similar to the box-counting method, the number of fracture center points is plotted against the size of the circle on logarithmic axes and the slope of the straight line yields the fractal dimension (Bunde and Havlin 1995). The sand-box technique measures different fractal characteristics and might yield different values than the box-counting method (Babadagli 2001). In addition, the spatial fractal dimension can be calculated using the distribution of fractures, or fracture intersections, instead of the fracture center points. Then, for the box-counting method, the number of fractures or the number of fracture intersections inside different-sized boxes is counted. Similarly, for the sand-box method, the number of fractures or fracture intersections inside different-sized circles is counted.

A total of 600 DFN with fractal dimensions ranging from $D = 1.0$ to 1.8 with 0.1 increments were created using a method described by Nakaya et al. (2003). The mirror images of the networks were used as well so a total of 1,200 different fracture networks were included in the library of networks. The positions of the fracture centers were selected according to the spatial fractal dimension D using the box-counting approach. At the ith iteration ($i = 1,2,3,\dots$), 2^{Di} boxes (rounded to the nearest integer) out of 4^i equally sized boxes were selected randomly. Thus, at the first iteration for $D = 1.4$, $2^{1.4 \times 1} = 3$ boxes were selected. Then, the procedure was repeated for $i = 2$, but

only the boxes selected during the previous iteration were available for selection in the successive iterations. In this study, four iterations were conducted and then the midpoints of all the boxes chosen during that last iteration were defined as fracture centers. As a result, the fracture centers form a self-similar structure and a Sierpinski gasket is obtained (Peitgen et al. 1990; Sierpinski 1915).

The dimension of the reservoirs was set as $1,000 \times 1,000 \ \mathrm{m}^2$ and the fracture lengths were determined according to the power-law exponent c and the maximum fracture length $l_{\max}$ using Eqs. (3)–(5). The power-law exponent was defined as 2.4 and the maximum fracture length was set as 600 m. The angles normal to the fractures were chosen to have two different distributions, both equally as likely to be chosen. The angles had a normal distribution with the mean either as 45° or as 135°, and with a standard deviation of 5°. The fracture aperture was defined by,

$$w = Cl^e \tag{7}$$

where w is the aperture and C is a constant. Olsen (2003) describes how this power-law equation was used to fit various fracture datasets of different sizes, usually with e equal to 0.4. Here, e was set as 0.4 and C as $0.002 \ \mathrm{m}^{3/5}$. Thus, the variation in fracture aperture is low, it varies by a factor close to 2 (depending on the spatial fractal dimension) and consequently the permeability calculated in Eq. (2) varies by a factor close to 4.

2.3 Fractional Connected Area

Fractional connected area is defined by the summed area of all clusters within a fracture network divided by the total sample area. The area of a cluster is delineated by the simplest polygon around the extremities of a fracture cluster (Fig. 1). Ghosh and Mitra (2009) concluded that FCA combined with a distribution of cluster sizes provides a complete measure of the connectivity of fractures within the system. FCA is also a good indicator of the overall fracture density and does not relate the cluster size to only the connectivity within the largest cluster as seen in other methods (Odling 1997). In fractured reservoirs, the connected area has high influence on the heat and mass transport in the system. Larger connected areas result in good connection and wider connected range with fluid traveling faster toward the producers, while fewer or smaller connected areas result in a poorer connection.

2.4 Inverse Analysis

An inverse analysis was used with the time history of the electric potential to estimate the connectivity of the fracture network. In inverse modeling the results of actual observations are used to infer the values of the parameters characterizing the system under investigation. In this study, the output parameters were the potential differences between wells as a function of time and the input parameter was the FCA of the reservoir. The objective function measures the difference between the model calculation (the calculated voltage difference between the wells) and the corresponding observed data measured at the reservoir, as illustrated in Fig. 2. An optimization algorithm was used to find the network with the most similar characteristics by proposing new
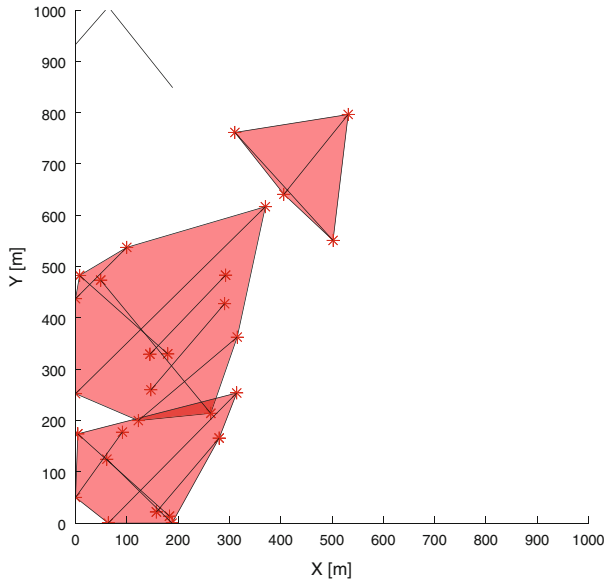
Fig. 1 Fractured reservoir with fractures shown in *black* and connected area in *red*

parameter sets that improve the match iteratively. In this case, a synthetic reservoir was compared to a library of 1,200 fracture networks to find the best match. A grid search algorithm was used due to the relatively small number of fracture networks so the reservoir response was compared to that of all the fracture networks in the library of networks. The best match was found using least squares, where the sum of the squared deviations between the electric curves for the true reservoir and the electric curves for the fracture networks is minimized. For every well pair in the reservoir, the following least squares criterion was calculated,

$$Q_j = \sum_{i=1}^{n}[y_i - f_i]^2 \tag{8}$$

where y_i is the electric potential difference between well pair j in the reservoir at time i and f_i is the corresponding electric potential for a fracture network in the library of networks. Then, the sum of Q_j for all well pairs was minimized to find the best match that has the lowest sum of Q_j. The relationship between the best match and the true fracture pattern was investigated by visually comparing the networks as well as by comparing the FCAs.

3 Results

3.1 Inversion of Time-Lapse Electric Potential Data

Conductive tracer simulations were performed and electric fields calculated for all the fractal fracture networks in the library of networks. For each of the networks, an
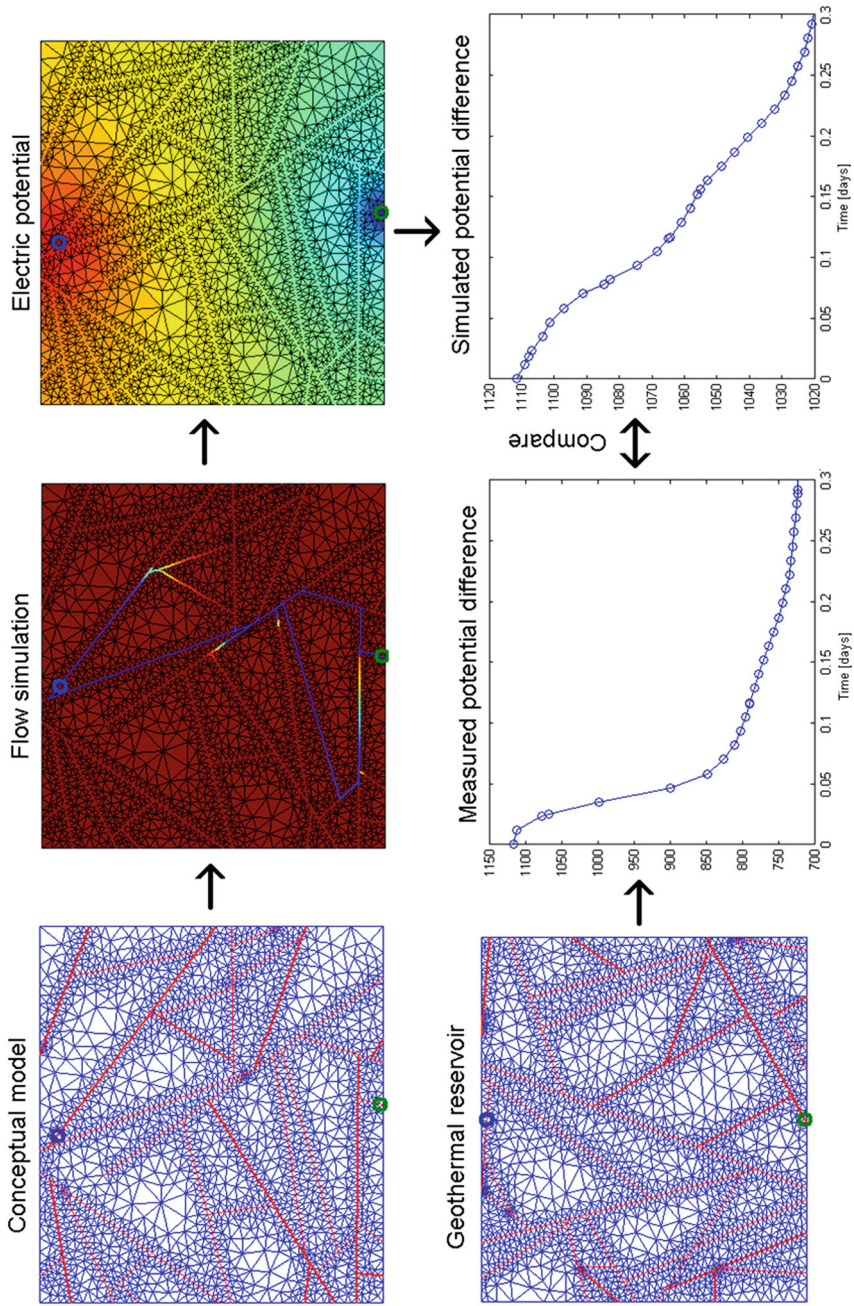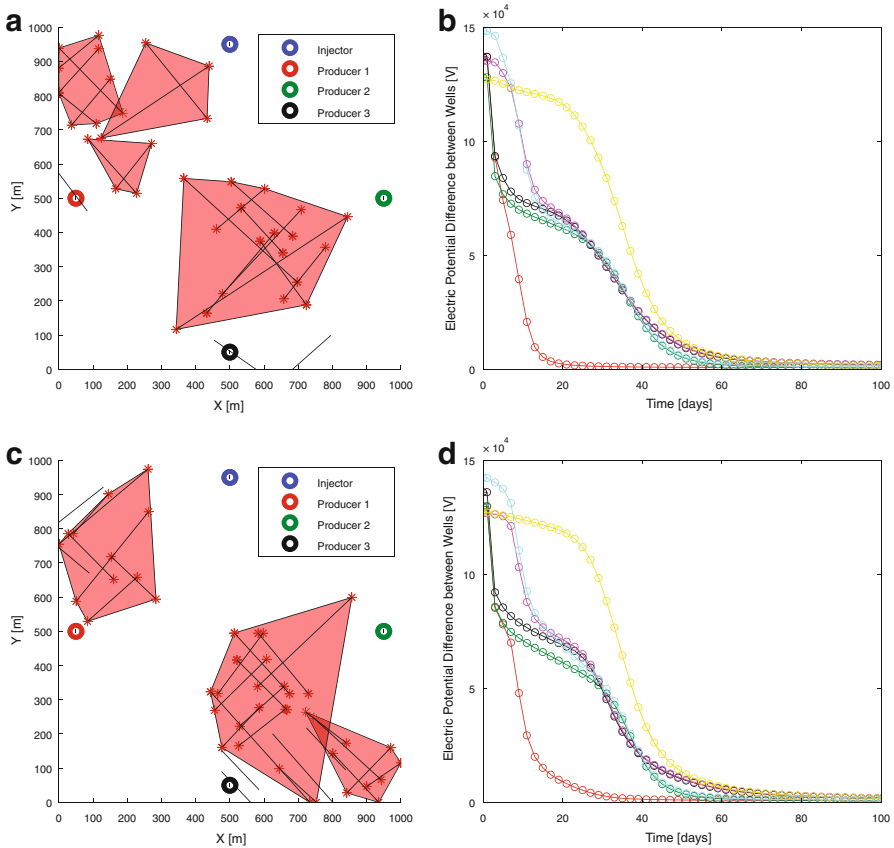
Fig. 2 Inverse analysis workflow

Fig. 3 **a** True reservoir, **b** electric potential difference between wells, **c** the best match for the true reservoir, and **d** electric potential difference for the best match

inverse analysis was performed to find the best match when comparing time-lapse electric potential data between all well pairs. As an example, GPRS was used to calculate the electric potential distribution for the reservoir in Fig. 3a. An electric current was set equal to 1 A at the injector and as −1 A at Producer 1 and the potential field was calculated based on the resistivity of the field at each time step. Then, the same procedure was repeated for all the other well pairs, with results shown in Fig. 3b. The electric potential curves calculated between the injector and Producer 1, injector and Producer 2, and injector and Producer 3, drop once the tracer is injected into the reservoir due to the low resistivity of the fluid injected. The fluid reaches the area between the other well pairs later so the corresponding electric potential curves decrease slower at the start. Then, the curve between the injector and Producer 1 drops relatively quickly and correctly indicates a good connection toward Producer 1.

Another interesting observation is that the curve between Producer 2 and Producer 3 drops relatively slowly despite a good connected area between these wells. That can be explained by looking at the tracer distribution, as shown in Fig. 4. Substantial
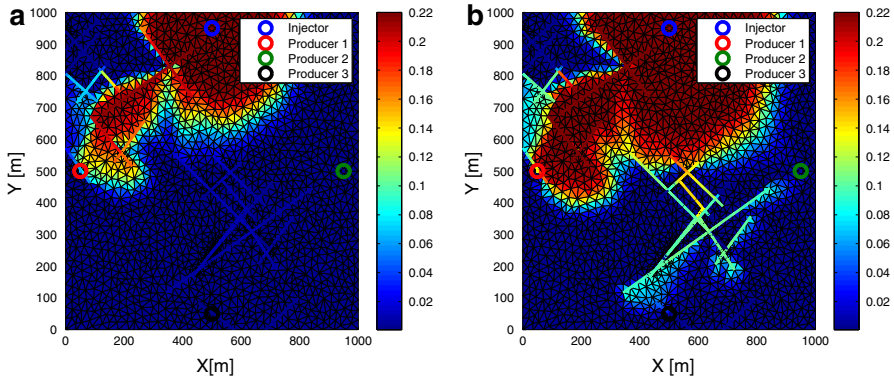
Fig. 4 Tracer distribution shown in *color* [kg$_{tr}$/kg$_{tot}$] after **a** 25 days, **b** 47 days
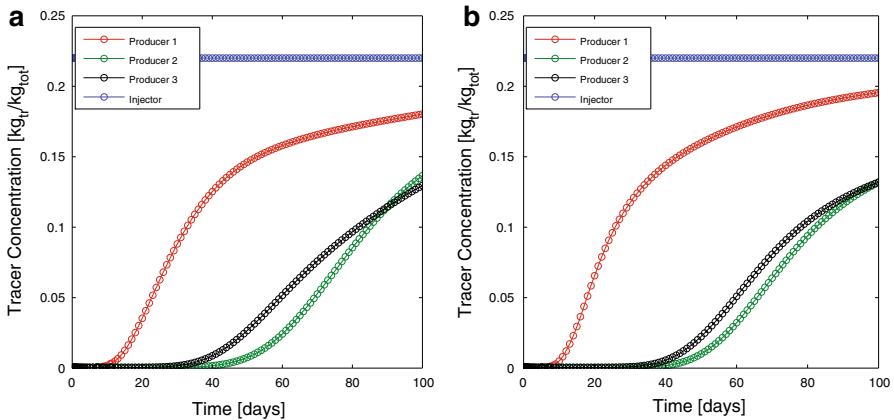

Fig. 5 **a** Tracer return curves for the true reservoir and **b** tracer return curves for the best match

amount of tracer flows toward Producer 1 because of the good connected area between the injector and Producer 1, and the tracer travels slower toward Producer 2 because there are no fractures in that area. After 25 days (Fig. 4a), the tracer has reached areas between all well pairs, but very little tracer has reached the area between Producer 2 and Producer 3, resulting in a slower drop in electric potential difference between these wells. After 47 days, the electric curves show similar electric potential differences between Producer 1 and Producer 3, and between Producer 2 and Producer 3. At that point, considerable amount of tracer has reached the fractures leading toward the area between Producer 2 and 3 (Fig. 4b). The simple tracer return curves at the producers were examined as well, shown in Fig. 5a. The tracer return curves also indicate a good connection toward Producer 1, with tracer in Producer 1 increasing after about 4 days. In addition, a poor connection is indicated toward Producer 2 with no tracer in Producer 2 until after about 16 days. The tracer reaches Producer 3 sooner, or after 12 days, because of the fractures located from the middle of the reservoir toward the lower right corner in Fig. 3a.

Next, the inverse analysis compared the time histories of the electric potential difference between well pairs for the true reservoir (Fig. 3a) to 1,200 other fracture networks. The fractal dimensions of the networks were ranging from $D = 1.0$ to 1.8 but other variables such as the size of the network, two principal fracture orientations, and relationship used for aperture were the same as for the true reservoir. A grid search algorithm was used to find the best match by minimizing the least squares criterion explained in Sect. 2.4. The chosen network (Fig. 3c) has curves for the electric potential (Fig. 3d) showing very similar behavior to the curves for the true reservoir (Fig. 3b). However, the tracer return curves for the best match show somewhat different behavior than for the true reservoir (Fig. 5).

The FCA of the network in Fig. 3c was compared to the FCA of the true reservoir. The results were FCA = 26.5 % for the reservoir, and FCA = 27.0 % for the best match. Thus, FCA matches very well for these two networks, indicating that FCA can be predicted in this example using this electric potential method.

The location of the connected areas is another similarity that can be seen between the best match and the true reservoir. In both cases, the connected fractures are located similarly in the upper left corners of Fig. 3a, c and the connected area reaching from the middle of the reservoir toward the area between Producer 2 and Producer 3 was also predicted correctly. However, the fracture network in Fig. 3c also has a connected area in the lower right corner of the figure, which is different from the true reservoir. The tracer travels from the injector toward the producer and might never reach the corners of the reservoir, so the electric potential gives very limited information about these areas.

Overall, the connected areas in Fig. 3a, c are similar, and the drops in electric potential between the well pairs correspond to the locations of the connected areas. These results indicate a good possibility of using electric potential calculations while injecting a conductive tracer into reservoirs to predict FCAs well as the locations of the connected area. In addition, the fractal dimensions of the two networks were similar, $D = 1.2$ for the real reservoir and $D = 1.1$ for the best match. Thus, it would be of interest to also investigate the possibility of using this method to predict the fractal dimension of fractal fracture networks.

3.2 Inversion of Tracer Return Data at Producers

Inverse analysis was performed again for the reservoir in Fig. 3a, but this time the objective function measured the difference between the model calculation of just the simple tracer return curves and the corresponding tracer return curves for the true reservoir. The objective was to compare the performance results of using the electrical approach to predict connected areas instead of only using tracer return curves. The best match when comparing the tracer return curves using a grid search algorithm is shown in Fig. 6. The time histories of the electric potential difference between he wells do not match as well as before when they were used to find the best match. However, in this case the tracer return curves (Fig. 7) match better than before. The fractal dimension is the same as for the reservoir, $D = 1.1$, but the estimated FCA for the network is 22.6 %, thus relatively smaller than for the true reservoir where FCA is
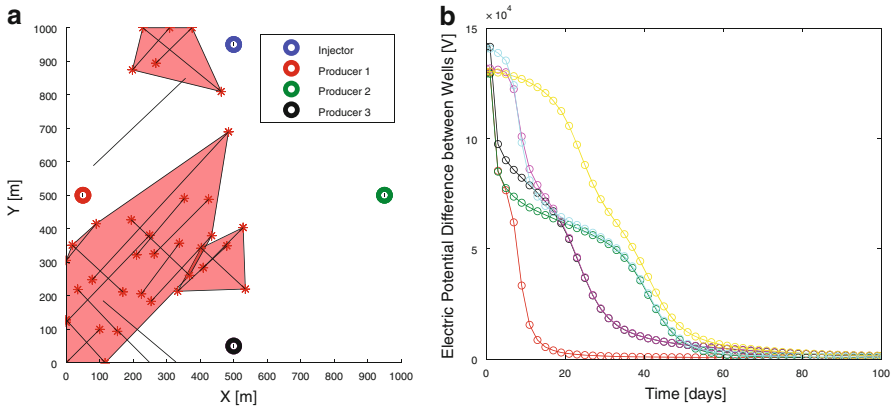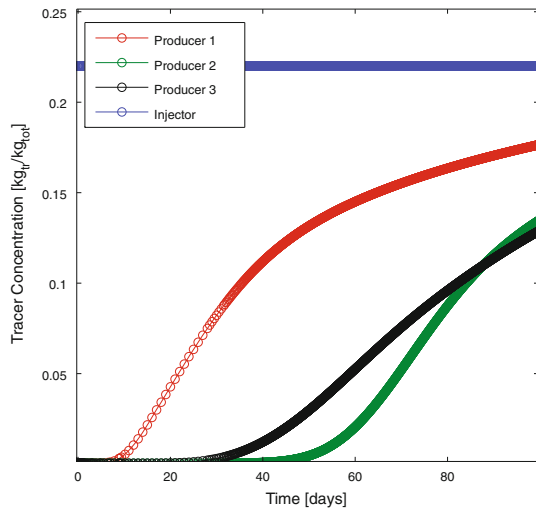
Fig. 6 **a** The best match when using tracer return curves and, **b** electric potential difference between well pairs

Fig. 7 Tracer return curves for the best match when using tracer return curves to find the best match

equal to 26.5 %. The fracture network (Fig. 6a) does have a connected area between the injector and Producer 1, but instead of having a connected area from the middle of the figure toward the lower right corner, this network has a connected area from the middle toward the lower left corner. Thus, tracer return curves indicate a connection in the middle toward Producer 3 but fail to determine the overall location of the largest connected area in the reservoir.

The same observation was also valid for another case studied previously (Magnusdottir and Horne 2013) and other examples shown in Fig. 8. The connected area for the reservoir in Fig. 8a is predicted well using electric potential curves (Fig. 8b) but the best match when using tracer return curves has more connected area to the left (Fig. 8c) instead of to the right (Fig. 8a). In addition, for the reservoir in Fig. 8d, the fracture network predicted using electric potential curves (Fig. 8e) is very similar
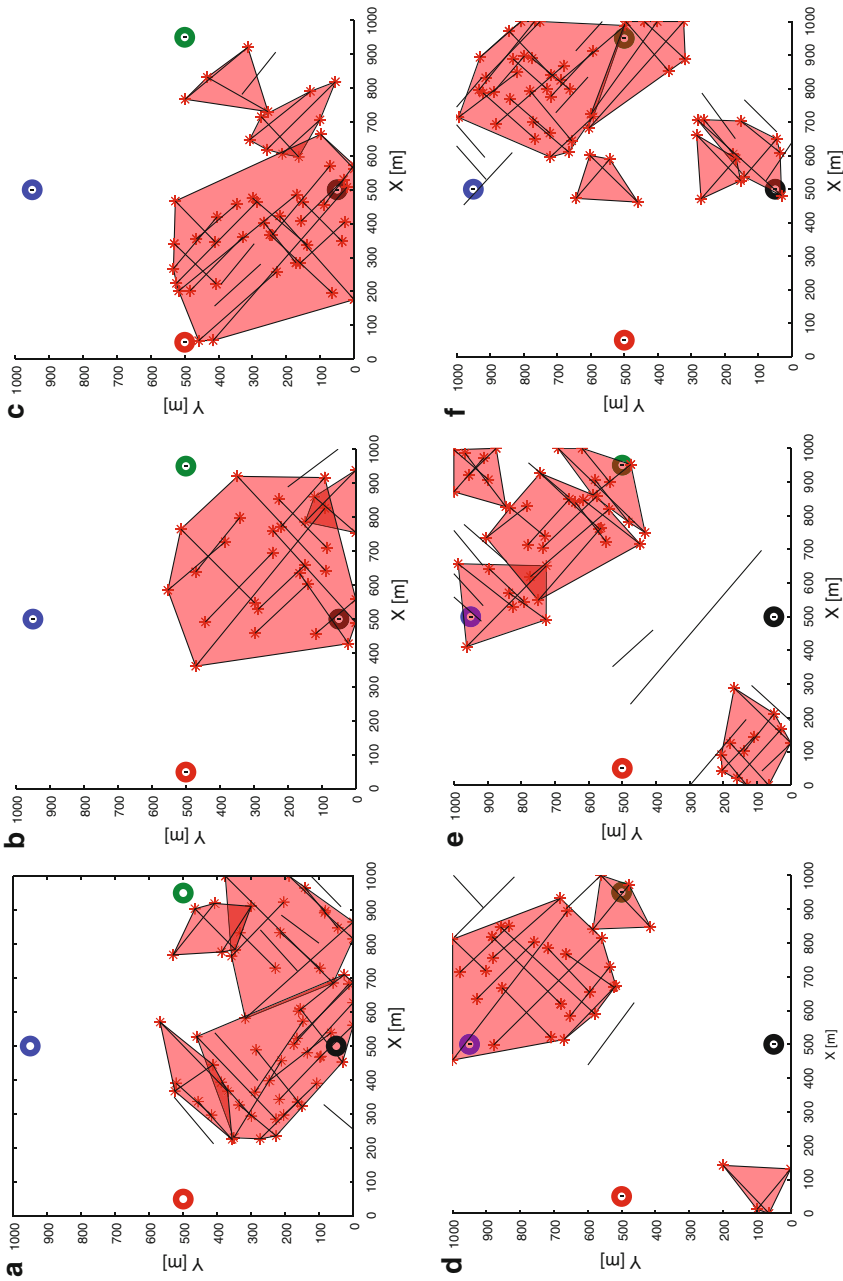
Fig. 8 **a** Reservoir 2, **b** best match using electric potential, and **c** best match using tracer return curves. **d** Reservoir 3, **e** best match using electric potential, and **f** best match using tracer return curves

to the reservoir but the tracer return results fail to predict the location of some of the connected areas correctly (Fig. 8f). These examples illustrate that the location of connected areas is predicted better using the electric potential measurements instead of using only the tracer return curves. The advantages of using the electric measurements include having more extensive data and being able to see the changes as the conductive fluid flows through the network even before it has reached the production wells.

4 Sensitivity Analysis

A sensitivity analysis was performed for all the well pairs in the reservoir to study the effect of FCA on the electric potential curves. Figure 9 shows the electric potential curves and the FCA represented by color for all well pairs. The electric potential difference between the injector and the other wells (Fig. 9a–c) drops quickly in the beginning because conductive tracer flows through the area between these wells as soon as it is injected at the injector. A correlation between the FCA and the electric potential differences between the injector and Producer 1 (Fig. 9a) is not clear and the same applies for the injector and Producer 2 (Fig. 9b). The electric potential depends on the local flow behavior between these wells and, therefore, depends on whether fractures happen to be located between these wells or not. Moreover, the following scenarios could occur causing the electric potential curves to not represent the FCA correctly:

 (i) Fractures in the reservoir increase the size of a connected area but the fractures are oriented perpendicular to the flow direction so they do not increase the flow rate of the tracer toward the producers.
(ii) Fractures are oriented in the flow direction but do not intersect other fractures. Thus, the fractures contribute to the flow but do not increase the FCA.

   However, a clear trend can be seen in the data for the well pair consisting of the injector and Producer 3, shown in Fig. 9c. The electric curves for high FCA (in red) are more likely to drop faster than electric curves for low FCA (in blue). High FCA corresponds to better connected reservoir with tracer likely to travel faster toward the producers, causing the electric potential to drop. This well pair covers almost the entire reservoir and, therefore, represents the regional connectivity of the reservoir better than the previous well pairs that represent more of a local flow behavior. Similar trends can be seen between the other wells in the reservoir (Fig. 9d–f), that is between Producers 1 and 3, Producers 2 and 3, and Producers 1 and 2. The time it takes for the tracer to reach the areas between these wells depends on the connectivity from the injector toward these areas. Thus, the electric differences depend not only on the fractures between the well pairs but also on the fractures forming paths from the injector toward these areas. In the inversion of the electric curves, all well pairs are used and the overall trend in the sensitivity analysis has shown a good correlation between the electric curves and FCA. A sensitivity analysis was also performed for the tracer return curves at the producers, as shown in Fig. 10 with color representing FCA. The tracer return curves were plotted for all the fracture networks in the library
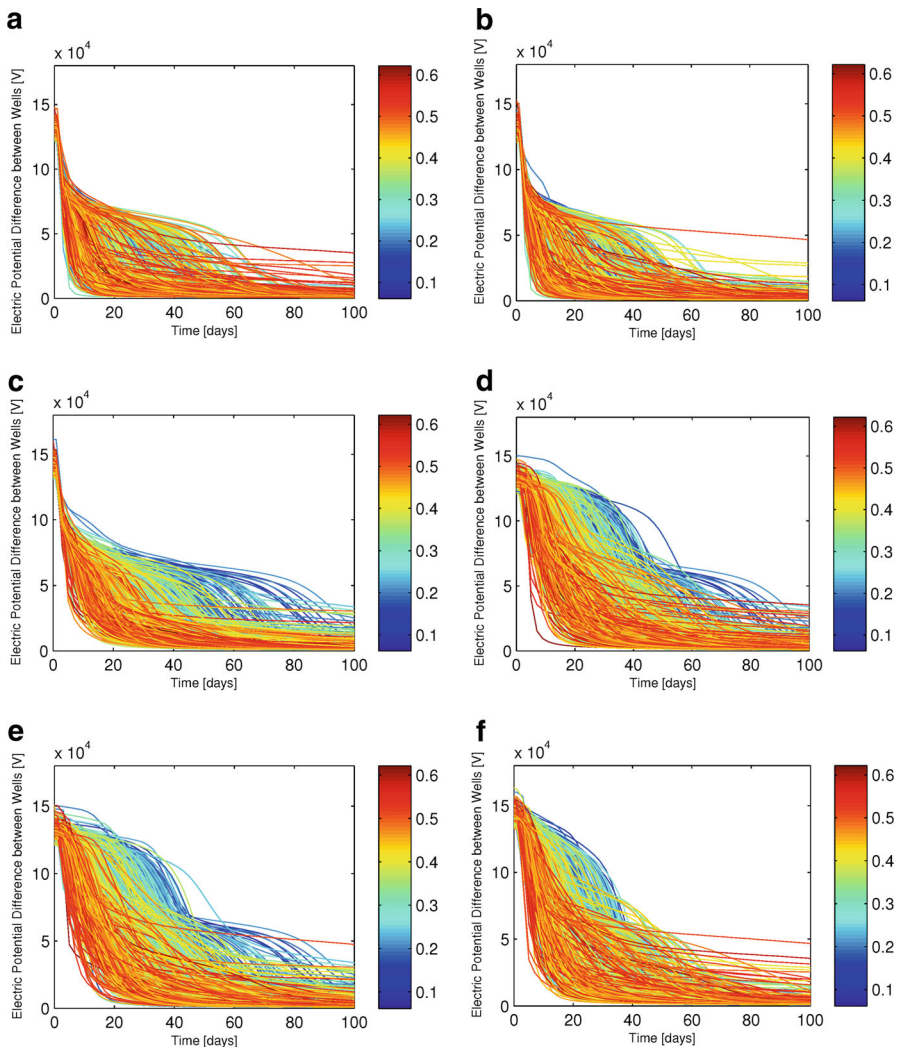
a

b

c

d

e

f

Fig. 9 FCA (*color*) with electric curves between **a** injector and Producer 1, **b** injector and Producer 2, **c** injector and Producer 3, **d** Producer 1 and Producer 3, **e** Producer 2 and Producer 3, and **f** Producer 1 and Producer 2

of networks to study the effect of FCA on the tracer return curves in comparison to the effects on the electric curves previously illustrated in Fig. 9. There is no clear trend for the tracer return curves at Producer 1 and Producer 2. There are curves with high FCA (in red) and with low FCA (blue) showing similar behavior because some fractures can be located between the injector and these producers despite the FCA being low. The tracer return curves at Producer 3 are more affected by the fractures in the whole reservoir and a slight trend with red curves (high FCA) increasing faster than blue curves (low FCA) can be noted.
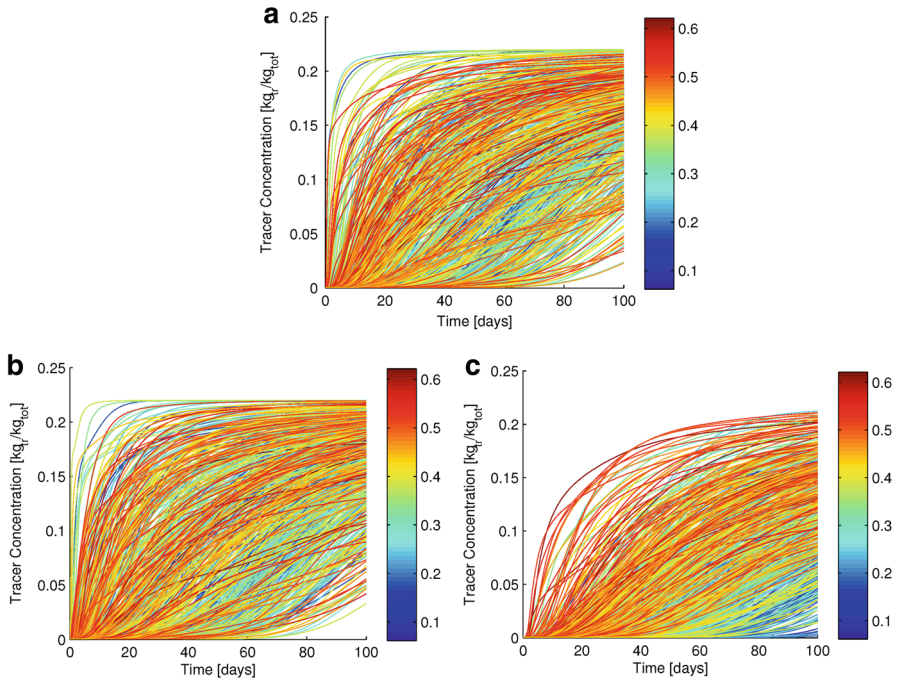
Fig. 10 FCA (*color*) with tracer return curves at **a** Producer 1, **b** Producer 2, and **c** Producer 3

5 Conclusion

The FCA of a hypothetical, fractured geothermal reservoir was estimated using electrical resistivity measurements with conductive fluid injection. Inverse analysis was used to match the time histories of the electric potential between the wells to the time histories of a library of fracture networks to find the best match. The reservoir and the best match had similar FCA and the connected areas had similar locations. For comparison, the inverse analysis was also performed matching the tracer return curves at the producers. The best match when using only the tracer return curves had a different FCA and the locations of the connected areas were somewhat different from the true reservoir. The same observation was made in other examples not included here.

A sensitivity analysis was performed to study the effects of FCA on the electric curves in comparison to the tracer return curves. The study demonstrated the feasibility of using time-lapse electric potential data with conductive fluid injection to estimate the connected area of the reservoir and its advantages over using only the tracer return curves.

References

Archie GE (1942) The electrical resistivity log as an aid in determining some reservoir characteristics. Trans AIME 146(99):54–67

Babadagli T (2001) Fractal analysis of 2-D fracture networks of geothermal reservoirs in south-western Turkey. J Volcanol Geotherm Res 112(1):1–4. doi:10.1016/S0377-0273(01)00236-0

Barton CC, Larsen E (1985) Fractal geometry of two-dimensional fracture networks at Yucca Mountain, southwestern Nevada. In: Proceedings of the international symposium on fundamentals of rock Joints, pp 77–84

Beall JJ, Michael C, Adams MC, Hirtz PN (1994) R-13 tracing of injection in The Geysers. Trans Geotherm Res Council 18:151–159

Berkowitz B (1995) Analysis of fracture network connectivity using percolation theory. Math Geol 27:467–483. doi:10.1007/BF02084422

Binley A, Cassiani G, Middleton R, Winship P (2002) Vadose zone flow model parameterisation using cross-borehole radar and resistivity imaging. J Hydrol 267(3):147–159. doi:10.1016/S0022-1694(02)00146-4

Binley A, Henry-Poulter S, Shaw B (1996) Examination of solute transport in an undisturbed soil column using electrical resistance tomography. Water Resour Res 32(4):763–769. doi:10.1029/95WR02995

Bunde A, Havlin S (1995) Fractals in science. Springer, Heidelberg

Cao H (2002) Development of techniques for general purpose simulators, PhD Thesis. Stanford University, CA, USA

Cassiani G, Brunoa V, Villa A, Fusi N, Binley A (2006) A saline trace test monitored via time-lapse surface electrical resistivity tomography. J Appl Geophys 59(3):244–259. doi:10.1016/j.jappgeo.2005.10.007

Chen J, Hubbard SS, Gaines D, Korneev V, Baker G, Watson D (2010) Stochastic estimation of aquifer geometry using seismic refraction data with borehole depth constraints. Water Resour Res 46:11. doi:10.1029/2009WR008715

Day-Lewis FD, Lane JW Jr, Harris JM, Gorelick SM (2003) Time-lapse imaging of saline-tracer transport in fractured rock using difference-attenuation radar tomography. Water Resour Res 39(10):1290. doi:10.1029/2002WR001722

Fossum MP, Horne RN (1982) Interpretation of tracer return profiles at Wairakei geothermal field using fracture analysis. Trans Geotherm Resour Council 6:261–264

Fukuda D, Akatsuka T, Sarudate M (2006) Characterization of inter-well connectivity using alcohol tracer and steam geochemistry in the Matsukawa vapor dominated geothermal field, Northeast Japan. Trans Geotherm Resour Council 30:797–801

Garambois S, Senechal P, Perroud H (2002) On the use of combined geophysical methods to assess water content and water conductivity of near-surface formations. J Hydrol 259(1):32–48. doi:10.1016/S0022-1694(01)00588-1

Garg SK, Pritchett JW, Wannamaker PE, Combs J (2007) Characterization of geothermal reservoirs with electrical surveys: Beowawe geothermal field. Geothermics 36(6):487–517. doi:10.1016/j.geothermics.2007.07.005

Ghosh K, Mitra S (2009) Two-dimensional simulation of controls of fracture parameters on fracture connectivity. AAPG Bull 93:1517–1533. doi:10.1306/07270909041

Axelsson G, Bjornsson G, Montalvo F (2005) Quantitative interpretation of tracer test data. Proceedings World geothermal congress, Antalya, Turkey, 24–29 April

Harthill N (1978) A quadripole resistivity survey of the Imperial Valley, California. Geophysics 43(7):1485–1500. doi:10.1190/1.1440910

Hochstein MP, Hunt TM (1970) Seismic, gravity and magnetic studies, broadlands geothermal field, New Zealand. Geothermics 2:333–346. doi:10.1016/0375-6505(70)90032-5

Holder DS (2004) Electrical impedance tomography: methods, history and applications. IPO, UK

Horne RN (1983) Effects of water injection into fractured geothermal reservoirs, a summary of experience worldwide. Trans Geotherm Resour Council 12:47–63

Hubbard SS, Chen J, Peterson J, Majer EL, Williams KH, Swift DJ, Mailloux B, Rubin Y (2001) Hydrogeological characterization of the south oyster bacteria transport site using geophysical data. Water Resour Res 37:2431–2456. doi:10.1029/2001WR000279

Irving J, Singha K (2010) Stochastic inversion of tracer test and electrical geophysical data to estimate hydraulic conductivities. Water Resour Res 46:11. doi:10.1029/2009WR008340

Jeannin M, Garambois S, Greegoire D, Jongmans D (2006) Multiconfiguration GPR measurements for geometric fracture characterization in limestone cliffs (Alps). Geophysics 71:85–92. doi:10.1190/1.2194526

Karimi-Fard M, Durlofsky LJ, Aziz K (2003) An efficient discrete fracture model applicable for general purpose reservoir simulators. SPE Reservoir Simulation Symposium, Houston

Keller GV, Frischknecht FC (1996) Electrical methods in geophysical prospecting. PressPergamon, Oxford

Koestel J, Kemna A, Javaux M, Binley A, Vereecken H (2008) Quantitative imaging of solute transport in an unsaturated and undisturbed soil monolith with 3-D ERT and TDR. Water Resour Res 44:12. doi:10.1029/2007WR006755

Lambot S, Antoinea M, van den Boschb I, Slobc EC, Vancloostera M (2004) Electromagnetic inversion of GPR signals and subsequent hydrodynamic inversion to estimate effective vadose zone hydraulic properties. Vadose Zone J 3:1072–1081. doi:10.2136/vzj2004.1072

Magnusdottir L, Horne RN (2012) Characterization of fractures in geothermal reservoirs using resistivity. Proceedings, 37th workshop on geothermal reservoir engineering. Stanford University, Stanford

Magnusdottir L, Horne RN (2013) Fracture connectivity of fractal fracture networks estimated using electrical resistivity. In: Proceedings, 38th workshop on geothermal reservoir engineering. Stanford University, Stanford

Main IG, Meredith PG, Sammonds PR, Jones C (1990) Influence of fractal flaw distributions on rock deformation in the brittle field. In: Knipe RJ, Rutter EH (eds) Geological society, London, Special Publications, vol 54.1, pp 81–96. doi:10.1144/GSL.SP.1990.054.01.09

Muskat M (1932) Potential distributions in large cylindrical disks with partially penetrating electrodes. Physics 2:329–364. doi:10.1063/1.1745061

Nakaya S, Yoshida T, Shioiri N (2003) Perlocation conditions in binary fractal fracture networks: applications to rock fractures and active and seismogenic faults. J Geophys Res 108:2348. doi:10.1029/94WR02260

Odling NE (1997) Scaling and connectivity of joint systems in sandstones from western Norway. J Struct Geol 19:1251–1271. doi:10.1016/S0191-8141(97)00041-2

Oldenborger GA, Knoll MD, Routh PS, LaBrecque DJ (2007) Time-lapse ERT monitoring of an injection/withdrawal experiment in a shallow unconfined aquifer. Geophysics 72:177–187. doi:10.1190/1.2734365

Olsen PA, Binley A, Henry-Poulter S, Tych W (1999) Characterizing solute transport in undisturbed soil cores using electrical and x-ray tomographic methods. Hydrol Process 13:211–221 doi:10.1002/(SICI)1099-1085(19990215)13:2<211:AID-HYP707>3.0.CO;2-P

Olson JE (2003) Sublinear scaling of fracture aperture versus length: an exception or the rule? J Geophys Res 108:2413. doi:10.1029/2001JB000419

Parra JO, Hackert CL, Bennett MW (2006) Permeability and porosity images based on P-wave surface seismic data: application to a south Florida aquifer. Water Resour Res 42:2. doi:10.1029/2005WR004114

Peitgen HO, Jurgens H, Saupe D (1990) Chaos and fractals. Springer, New York

Rouleau A, Gale JE (1985) Statistical characterization of the fracture system in the Stripa granite. Int J Rock Mech Mining Sci Geomech Abstr 22(6):53–367. doi:10.1016/0148-9062(85)90001-4

Shaw HR, Gartner AE (1986) On the graphical interpretation of paleoseismic data. US Geological Survey Open-File Report, pp 86–394

Shewchuk JR (1996) Triangle: engineering a 2D quality mesh generator and delaunay triangulator. Applied Computational Geometry Towards Geometric Engineering, vol 1148, pp 203–333. doi:10.1007/BFb0014497

Shook GM (2001) Predicting thermal breakthrough in heterogeneous media from tracer tests. Geothermics 30(6):573–589. doi:10.1016/S0375-6505(01)00015-3

Sierpinski W (1915) Sur une courbe dont tout point est un point de ramication. C R Acad 160:302

Singha K, Day-Lewis FD, Moysey S (2007) Accounting for tomographic resolution in estimating hydrologic properties from geophysical data. Geophysics 171:227–241. doi:10.1029/171GM16

Singha K, Gorelick SM (2005) Saline tracer visualized with three-dimensional electrical resistivity tomography: field-scale spatial moment analysis. Water Resour Res 41:5. doi:10.1029/2004WR003460

Singha K, Gorelick SM (2006) Hydrogeophysical tracking of three-dimensional tracer migration: the concept and application of apparent petrophysical relations. Water Resour Res 42:6. doi:10.1029/2005WR004568

Slater L, Binley AM, Daily W, Johnson R (2002) Cross-hole electrical imaging of a controlled saline tracer injection. J Appl Geophys 44:85–102. doi:10.1016/S0926-9851(00)00002-1

Stauffer D (1985) Introduction to percolation theory. Taylor and Francis, London

Ucok H, Ershaghi I, Olhoeft GR (1980) Electrical resistivity of geothermal brines. J Petroleum Technol 32(4):717–727. doi:10.2118/7878-PA

Wu X, Pope GA, Shook GM, Srinivasan S (2008) Prediction of enthalpy production from fractured geothermal reservoirs using partitioning tracers. Int J Heat Mass Transfer 51(5):1453–1466. doi:10.1016/j.ijheatmasstransfer.2007.06.023

Xu C, Dowd PA, Mardia KV, Fowell RJ (2006) A connectivity index for discrete fracture networks. Mathem Geol 38:611–634. doi:10.1007/s11004-006-9029-9

Yeh TCJ, Liu S, Glass RJ, Baker K, Brainard JR, Alumbaugh DL, LaBrecque D (2002) A geostatistically based inverse model for electrical resistivity surveys and its applications to vadose zone hydrology. Geophysics 38(12):14-1:1413. doi:10.1029/2001WR001204